Polymer Chemistry

Electrochromism of Alkylene-Linked Discrete Chromophore Polymers with Broad Radical Cation Light Absorption

SCHOLARONE™
Manuscripts

Electrochromism of Alkylene-Linked Discrete Chromophore Polymers with Broad Radical Cation Light Absorption

Dylan T. Christiansen,[†] David L. Wheeler,[‡] Aimée L. Tomlinson,[‡] and John R. Reynolds*[†]*

[†]School of Chemistry and Biochemistry, School of Materials Science and Engineering, Center for Organic Photonics and Electronics, Georgia Tech Polymer Network, Georgia Institute of Technology, Atlanta, GA, 30332

[‡]Department of Chemistry/Biochemistry, University of North Georgia, Dahlonega, GA 30597

ABSTRACT: This study focuses on examining the design principles of creating multi-heterocycle chromophores with a discrete conjugation length, which absorb ultraviolet light in the neutral state, and upon oxidation absorb throughout a broad spectral range in the visible. In this analysis, three discrete-length chromophore polymers with alkylene linkers were examined via time dependent DFT, synthesized via direct heteroarylation polymerization, and the electrochromic properties of their thin film characterized. Using a feedback loop of theoretical calculations with design and synthesis, we elucidate how steric interactions can be used to control the absorption of the neutral and oxidized states of these discrete chromophore polymers. We show that systems with high inter-ring strain can be used to increase the molar absorptivity of the charged state by forming multiple radical cation states on a

single discrete chromophore. We also demonstrate the challenges of electrochemical redox reversibility in the solid state in these systems, while they maintain their chemical redox reversibility.

Introduction

When considering materials that can switch between colored and transmissive states, redox active electrochromic polymers have structurally controlled optical and switching properties that offer a wide variety of applications.[1] These applications include full color passive and active displays, energy saving tinted windows, switchable mirrors, and dimmable visors, goggles and glasses for military and/or recreational use. Organic electrochromic polymers (ECPs) offer some advantages over their inorganic counterparts in that they are solution processable under ambient conditions, lightweight, and flexible, while providing a fine degree of structurally induced color control.[2–4] Polymeric π-conjugated materials used in electrochromic and other optoelectronics applications have seen vast improvements in performance over recent years due to an increased understanding of their interactions with electrodes, solution processing characteristics, and thin film morphologies.[5–8]

The history of research in fully conjugated cathodically coloring ECPs has yielded materials that span the entire color palette.[9] These polymers can be spray cast to form vividly colored films that upon oxidation become highly transmissive in the visible region. Recently, approaches towards creating black-to-transmissive electrochromic polymeric materials have been investigated through the generation of broadly absorbing copolymers or via solution mixing of polymeric inks.[10–17] The latter of the two approaches allows for finer control, more accurate reproducibility, and higher contrast through the mixing of cyan, magenta, and yellow materials to create a broadly absorbing blend.

Although cathodically coloring polymers provide precise control of color and electrochemical properties, they have an inherent challenge when it comes to making improvements in contrast, which is explored in **Figure 1**.[18] In the charge neutral state (black trace) conjugated ECPs absorb in the visible with a single π-π* transition (exceptions include donor-acceptor systems that have dual band

absorbances and some random copolymers that have a manifold of absorbances).[19] The oxidation states

for a single polymer chain in solution consists of dual transition polarons and single transition

bipolarons with discrete absorbances (red and blue traces, respectively) at longer wavelengths than the

neutral polymer. In the solid-state, charged states interact with one another creating a complex system

where selection rules are relaxed and more transitions are possible. This leads to the characteristically

broad profile for the oxidized states of fully conjugated ECPs, as seen in the green trace. An asymmetric

absorption throughout the visible region, absorbing more low energy red light and transmitting more of

the higher energy blue light, manifests itself in such a way that highly oxidized states of conjugated

ECPs exhibit a transmissive grey-blue hue. Reaching a color neutral and fully transmissive oxidized

state across the entire visible spectrum is difficult due to this relaxation of the selection rules allowing

broad light absorption in these materials.
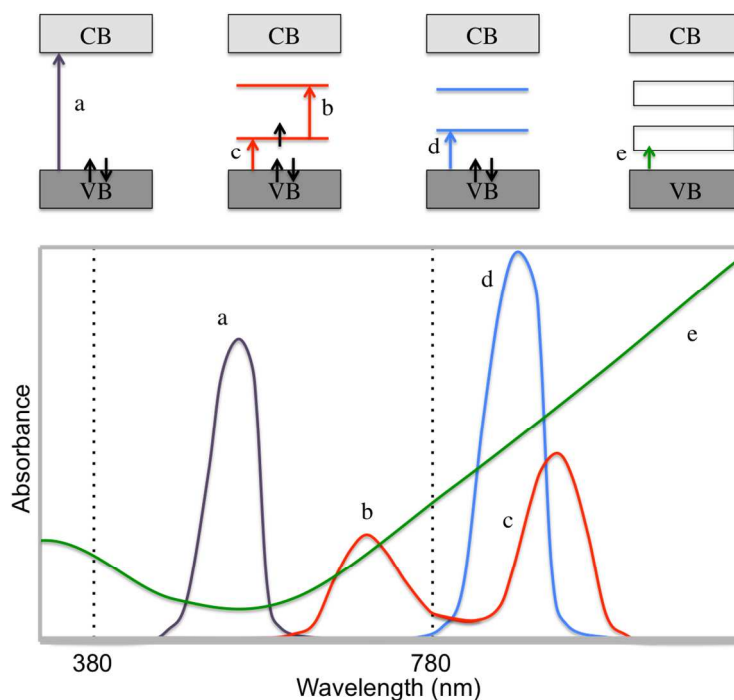
Figure 1. Electronic structures of allowed transitions in conjugated electrochromic polymer chains as a

function of oxidation state: (a) a neutral polymer, (b and c) a polymer carrying a polaron, (d) a polymer

carrying a bipolaron, (e) a polymer or assembly of polymer chains with a high concentration of polarons

and bipolarons (intrachain or interchain polaron network), a chain or assembly of chains with a high

concentration of bipolarons (intrachain or interchain bipolaron bands). A representation for absorbance spectra of these transitions is illustrated at the bottom. (Adapted and modified from Reference 18)

A class of materials that has potential to avoid this particular contrast issue is anodically coloring electrochromic (ACE) materials.[20–26] These materials have a neutral state absorption that is localized in the UV and, upon oxidation form broad charged-state absorptions that can be dominant across the visible. The most successful anodically coloring polymers prepared to date are made based on 3,4-dioxypyrroles or triphenylamines.[27–36] However, each of these materials have their own disadvantages. For 3,4-dioxypyrrole systems, the lack the facile chemistry for incorporation into alternating copolymers limits their synthetic flexibility. These polymers also contain charged states that mainly absorb in the near-IR with minimal absorbance of blue light.[37] The triphenylamine polymers tend to undergo oxidation at potentials well over 1 V vs. Ag/Ag^+ which is higher than most fully conjugated, cathodically coloring electrochromic systems, making the cation state more reactive and the materials less stable to repeated redox switching.[38,39] These issues detract from the ability to utilize these polymers in blends to create transmissive switching to broadly absorbing black mixtures.

Here, we explore anodic coloration as a methodology for designing electrochromic polymers where we avoid the NIR tailing observed in cathodically coloring ECPs as demonstrated in **Figure 2**. These materials are designed to have electron rich, conjugated chromophores of discrete length, which have wide optical gaps absorbing specifically in the UV in their neutral state with minimal tailing into the visible in the colorless state. This can be seen by the solid curve in **Figure 2**. Upon oxidation to the radical cation state, short conjugation lengths maintain a high-energy absorption relative to fully conjugated polymer systems, moving the absorbance into the visible region (380-780 nm). This broad dual band absorbance is denoted by the dashed curve. In order to effectively design these materials as effective high contrast electrochromes, a fundamental understanding must be developed on how conjugation length, electron-rich character, and steric strain control the redox potential for switching to, and the absorption characteristics of, the radical cation state.
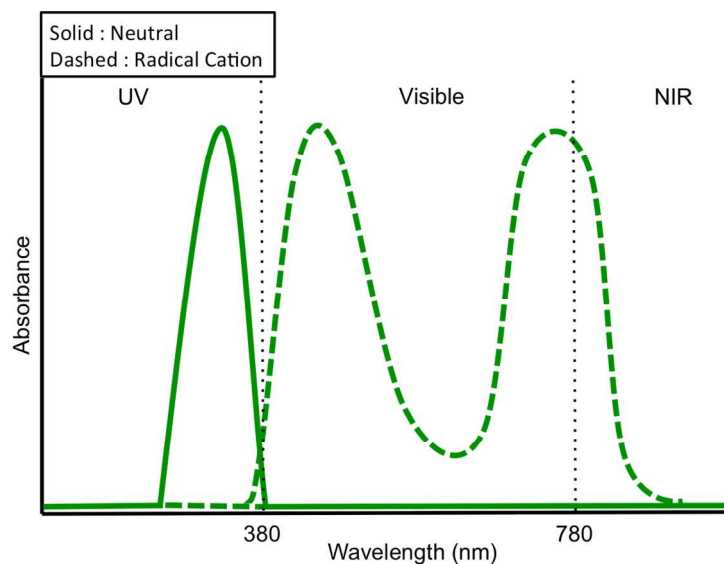
Figure 2. Theoretical spectra for an ideal anodically coloring material with a UV absorbing neutral state and broadly absorbing radical cation state.

Towards this aim, a family of polymers with discrete length, π-conjugated chromophores was synthesized to give insight into these fundamental structure-property relationships (repeat unit structures in **Scheme 1**) with the goal of providing design characteristics for anodically coloring electrochromic polymers. This family of chromophores models the interplay between increasing chromophore conjugation length and interring steric strain and examines the absorption characteristics of both the neutral and radical cation states of the chromophores, while using electron rich moieties to maintain a low oxidation potential. Polymers containing discrete chromophores systems have been explored as an approach to electrochromics before. [40,41] In these experiments both chromophores in a polymer chain as well as conjugated chromophore side chains were examined showing electrochemical activity and optical switching upon oxidation/reduction.
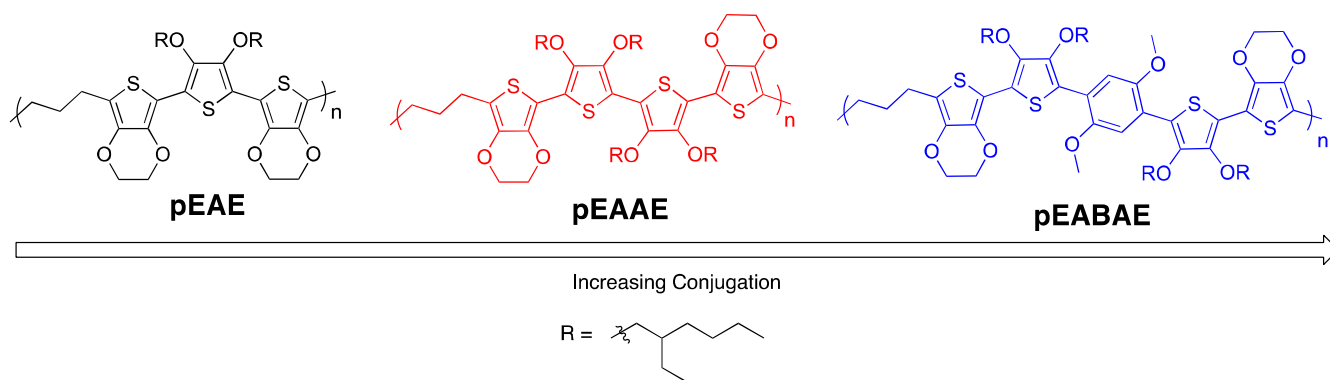
Scheme 1. Repeat unit structures for a family of dioxythiophene based discrete length chromophore polymers being investigated in order of increasing conjugation.

Results and Discussion

Quantum Chemical Calculations – Interring Strain. To elucidate the influence of structural modification on the electronic and spectral properties of the chromophores, density functional theory (DFT) was utilized. Previously, we have shown mPW1PBE functional paired with the cc-PVDZ basis set (detailed information for each included in the Supplemental Information) provides excellent correlation of optical properties to experimental spectra for dioxythiophene-containing systems.[42] To mimic the environment each system experiences during experimental data collection, all computations were performed with the incorporation of the conductor polarizable calculation model (CPCM) using dichloromethane as the applied dielectric. For each ECP, this level of theory was applied to a single chromophore in its neutral, radical cation, and dication states to predict changes in the optimized ground state geometry upon oxidation. Time-dependent DFT (TD-DFT) calculations were then performed on these geometries to simulate UV-Vis spectra, which provided insight on tuning the absorptivity of chromophores. Chromophores with high energy π-π* transitions were designed by restricting the conjugation length to three, four, and five heterocycles while also maintaining a low oxidation potential.

The impact of interring strain between neutral and oxidized states was examined utilizing the first set of ter(heterocycle) systems shown in **Scheme 2**. Each chromophore contained terminal groups of

methyl-capped 3,4-ethylenedioxythiophene (**E**) and a distinct middle heterocycle: either a branched

alkyl ether functionalized 3,4-propylenedioxythiophene (**P**) or a 3,4-bis(2-ethylhexyloxy)thiophene (**A**).

By changing the identity of the middle heterocycle, the proximity of the alkoxy-chains relative to the

conjugated backbone varied as a function of distance, while the number of π-electrons in the

chromophore remained unchanged.   The degree of interring strain was determined by observing the

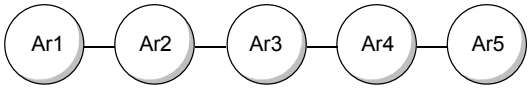changes in dihedral angles between the terminal and middle heterocycles in each chromophore.
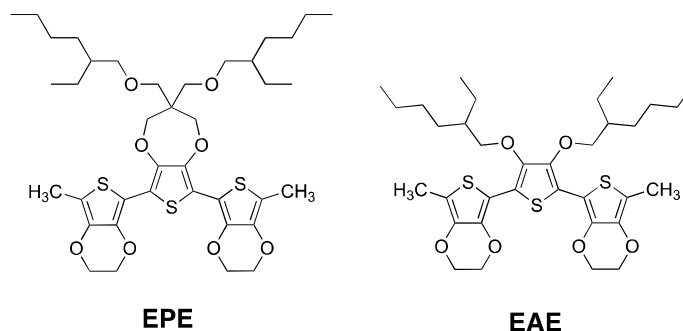
Scheme 2. Methyl-terminated ter(heterocycles) evaluated in the strain study.

The results of the structural data for these ter(heterocycles) from the optimized geometry are collated in

Table 1. The rings were numbered in each chromophore, and the interring bond lengths, dihedral

angles, and first excited state energies (TD-DFT HOMO-LUMO gap) were measured.   Examining the

dihedral angle measurements, it is clear that the proximity of the 2-ethylhexyl solubilizing groups affect

the degree of conjugation as the HOMO-LUMO gap for **EAE** is 0.68 eV higher than **EPE**.   Since the

solubilizing chains are farther from the backbone of the chromophore in **EPE**, all three heterocycles

remain in excellent conjugation with one another, independent of the charged state.   However, for the

neutral **EAE** chromophore, only two of the three heterocycles are found to be exceptionally planar

(175.2°) while the third heterocycle remains orthogonal (91.5°). Upon oxidation, the **EAE** chromophore

becomes increasingly planar, reducing the orthogonal character (178.8° and 164.4°).   The oxidized

chromophores exhibit more quinoidal character as the bond length between heterocycles decrease by
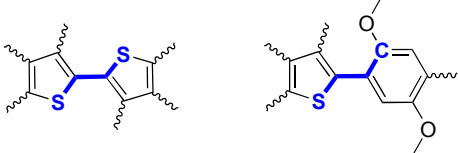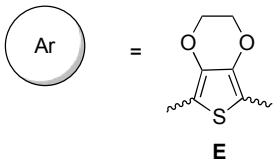
~0.03 Å.

Table 1. Structural data for all target oligomers in this study. The figure key shows how rings and dihedral angles are numbered and symbolized in the table.
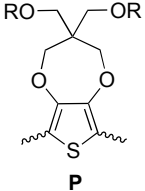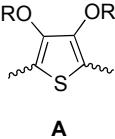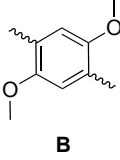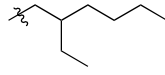

	EPE		EAE		EAAE		EABAE	
	neutral	polaron	neutral	polaron	neutral	polaron	neutral	polaron
First-Excited State Energy (eV)	3.00	-	3.68	-	3.15	-	3.64	-
Ar1-Ar2 (Å)	1.44	1.41	1.46	1.41	1.44	1.41	1.46	1.41
Ar2-Ar3 (Å)	1.44	1.41	1.44	1.41	1.46	1.41	1.47	1.44
Ar3-Ar4 (Å)	-	-	-	-	1.45	1.41	1.47	1.44
Ar4-Ar5 (Å)	-	-	-	-	-	-	1.46	1.42
Ar1-Ar2 Dihedral	177.2	178.3	91.5	164.4	174.8	179.7	86.8	167.3
Ar2-Ar3 Dihedral	177.2	178.3	175.2	178.8	111.6	151.4	121.5	137.7
Ar3-Ar4 Dihedral	-	-	-	-	174.8	179.7	125.6	132.5
Ar4-Ar5 Dihedral	-	-	-	-	-	-	83.7	169.1

The structural models for the ter(heterocycles) are corroborated with the analysis of the calculated UV-Vis spectra as depicted in **Figure 3**. The absorption of **EPE** (λ_{max} = 413 nm) occurs extensively throughout the visible due to a lack of interring strain, while the converse is observed for **EAE** (λ_{max} = 337 nm). This comparative blue shift is attributed to the effective conjugation between only two of the three heterocycles in **EAE** (**Figure 4**). While the neutral spectra for each chromophore are unique, the radical cation spectra have surprisingly similar characteristics (energies and band widths). As predicted from **Figure 1**, there are two peaks in the radical cation spectra for each chromophore, the higher energy

peak indicative of the singly occupied molecular orbital (SOMO) to LUMO transition (b) and the lower

for SOMO-n to SOMO (c) (note only the high energy radical cation peak is shown in **Figure 3**). For the

SOMO to LUMO transitions, there is only a 7 nm difference between the peak maxima of each

chromophore. In the case of the lower energy transitions (refer to **Figure S2**), the peak maxima occur at

831 nm (**EPE**) and 809 nm (**EAE**) with similar oscillator strengths. These spectra demonstrate the

ability to control the neutral state absorbance while producing nearly the same oxidized spectra. Thus,

this theoretical experiment guides the focus of synthetic efforts towards highly strained acyclic systems

to produce colorless neutral chromophores.
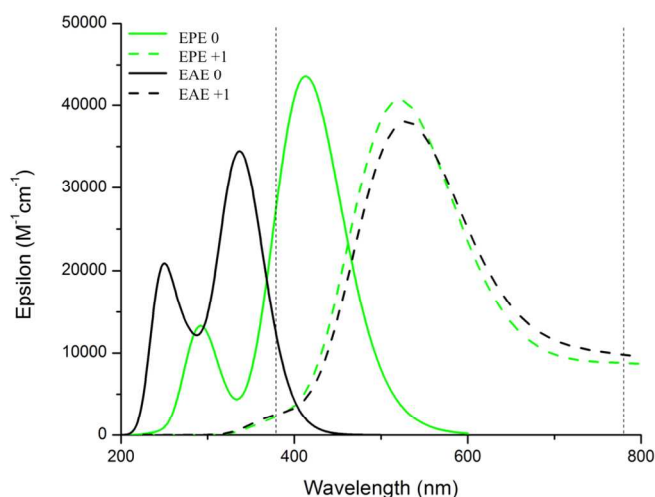
Figure 3. UV-Vis spectra of **EPE** and **EAE** in the neutral (solid) and radical cation (dashed) states.
Vertical dotted lines indicate the visible range of 380-780 nm.

Quantum Chemical Calculations – Conjugation vs. Strain. We next focused our attention on

designing materials that absorb little to no visible light in the neutral state, but exhibit broad absorbance

upon oxidation. Through the incorporation of excess strain, the absorption of a chromophore is driven

into the UV-region. Additionally, increasing the conjugation by utilizing more aromatic systems in a

single chromophore facilitates the polaronic spectrum to absorb broadly in the visible. To this end, the

methyl-capped four and five ring chromophores shown in **Scheme 3** were explored where the latter

included dimethoxybenzene (**B**), which offers a high degree of strain and an inherently wider optical gap than thiophene-based systems due to an increased aromaticity.
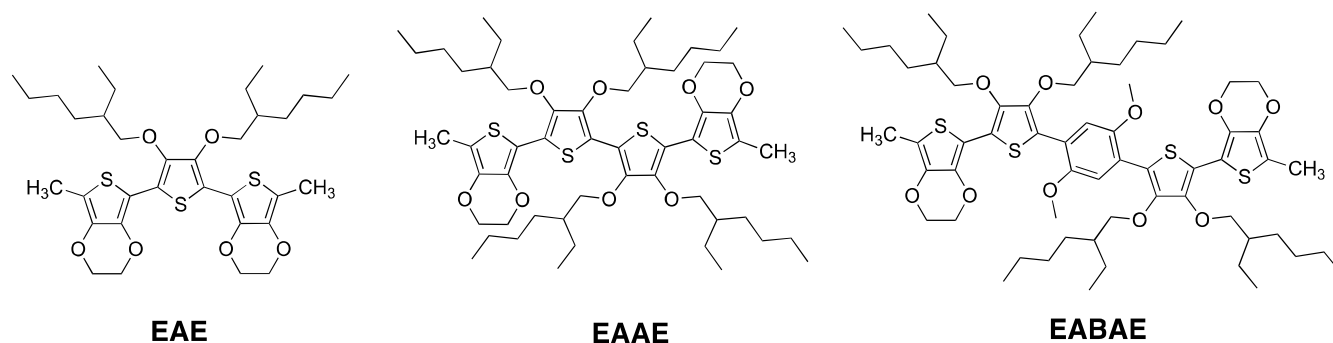
Scheme 3. Structural scheme depicting the chromophores evaluated in the conjugation study.

Examining the neutral structural data in **Table 1**, it is evident that the **EABAE** system contains a significant amount of strain as the dihedral angles between each chromophore ranges between 83.7° - 125.6°, limiting the conjugation along the backbone. For **EAAE**, the dihedral angles between each **E** and **Ac** heterocycles are exceptionally planar (174.8°) while the dihedral angle between the two **Ac** units exhibit considerable strain (111.6°). These effects are further reflected in the calculated UV-Vis spectra (**Figure 5**). In comparison to the neutral, low-energy peak of **EAE**, the peak for **EAAE** is red-shifted by 133 nm into the visible region making this chromophore undesirable. However, in the case of the **EABAE**, the simulated spectrum produces a single peak, which aligns with the low energy peak of **EAE**. The calculations for **EABAE** showed the primary transition occurs from HOMO → LUMO with an oscillator strength of 0.95. All other transitions had oscillator strengths less than 0.11 and were therefore negligible in the absorption spectrum. Upon closer analysis of the frontier molecular orbitals (**Figure 4**), the majority of electron density in the ground-state is delocalized on the **EAB** portion of the chromophore; in essence half of the molecule. Due to the increased strain along the backbone, the effective conjugation along the chromophore is compromised, producing an optical gap comparable to that observed in **EAE**.
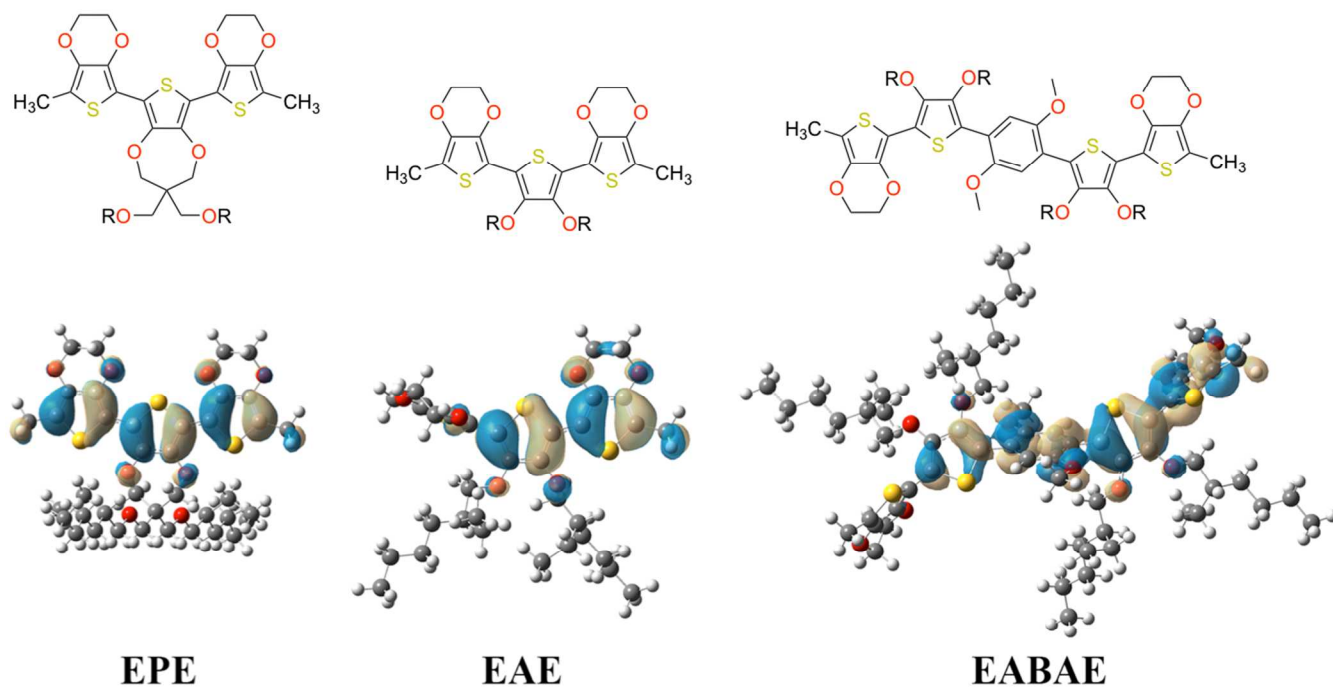
Figure 4. Frontier molecular orbital diagrams detailing the HOMO of the neutral, ground-state energy of **EPE**, **EAE**, and **EABAE**.

Upon oxidation, all three chromophores become dramatically planar. For the **EAAE** chromophore, the **E-A** dihedrals planarize to 179.7° and the **A-A** dihedral shifts to 151.4°. Similarly, for **EABAE**, the range of dihedral angles decreases to 132.5° to 169.1°. Each oxidized chromophore is found to absorb significantly in the visible, particularly **EAE** with a peak maximum at 527 nm and broad absorption leading into the near IR. **EAAE** exhibits a broad absorption leading into the near IR due to a prominent red-shift of 118 nm. Finally, **EABAE** has a single visible peak comprised of two excited states (474 nm and 514 nm, **Figure S3k**), which is blue-shifted to **EAE**. Upon closer examination of all spectra, **EAE** and **EABAE** are the most promising electrochromic materials due to their high transmissivity coupled with visible absorption in their neutral and radical cation states, respectively.
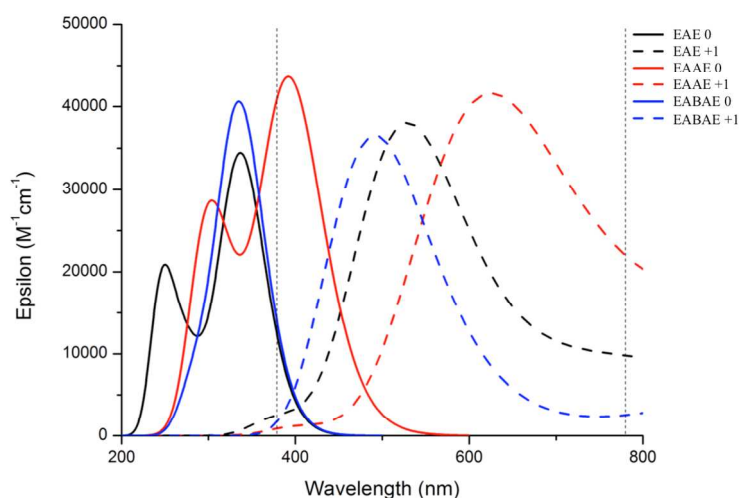
Figure 5. Calculated UV-Vis spectra of the neutral (solid) and radical cation (dashed) states of **EAcE**, **EAAE**, and **EABAE**. Vertical dotted lines indicate the visible range of 380-780 nm.

Synthesis. The target polymers in **Scheme 1** were synthesized as described in **Scheme 4**. By lithiation of 3,4-ethylenedioxythiophene (EDOT) and subsequent quenching with propylene-1,3-ditosylate the dihydrin monomer (**E~E**) was synthesized. The polymerizations were carried out via a direct heteroarylation mechanism with the respective dibromo monomers to create the family of polymers with discrete chromophores. The polymers were purified via Soxhlet extraction and the repeat unit structure confirmed using ^{1}H and ^{13}C NMR and elemental analysis. Polymer molecular weights were analyzed with gel-permeation chromatography (GPC) in CHCl$_3$ at 40°C and the number average molecular weights and dispersity (M_n, Đ) relative to polystyrene standards are as follows: **pEAE** (14.8 kDa, 2.0), **pEAAE** (18.5 kDa, 1.8), **pEABAE** (9.7 kDa, 2.0) (**Figure S1**). Synthetic procedures for **E~E** can be found in the supporting information along with characterization results on ^{1}H-NMR, ^{13}C-NMR, mass spectrometry, elemental analysis, and GPC.
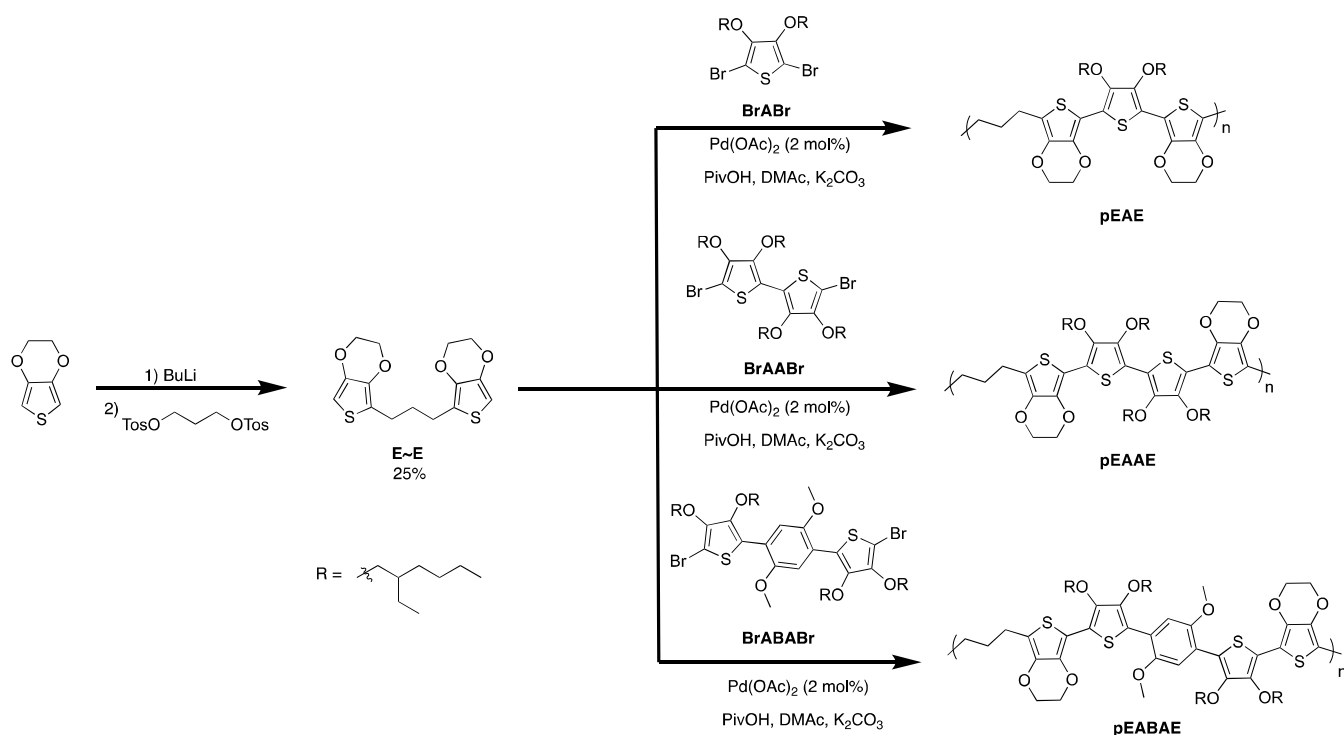
Scheme 4. Synthetic scheme outlining the synthesis of the target polymers. (PivOH = pivalic acid and DMAc = *N,N*-dimethylacetamide)

Electrochemical and Optical Properties. All electrochemical measurements were performed on films that were drop cast (3 µL of 2 mg/mL solutions in $CHCl_3$) on glassy carbon electrodes in 0.5 M tetrabutylammonium hexafluorophosphate (TBAPF$_6$). Cyclic voltammetry (CV) and differential pulse voltammetry (DPV) were used to probe the redox properties of the target polymers as illustrated by the results in **Figure 6**. The onsets of oxidation measured via DPV were 0.13 V, 0.16 V, and 0.25 V for **pEAE**, **pEAAE**, and **pEABAE**, respectively. This is counter-intuitive to the idea that increasing conjugation causes a raising of the HOMO and thus lower ionization potential, but is corroborated by the DFT calculations predicting this larger energy barrier to planarize for the **A-A** bond (**Table 1**). The strong **A-A** steric interaction in **pEAAE** leads to a large planarization energy, which leads to a similar oxidation potential despite the increase in conjugation length. As predicted by the DFT calculations this

13

steric effect is even more intense in the case of the **pEABAE** leading to an even higher oxidation

potential.
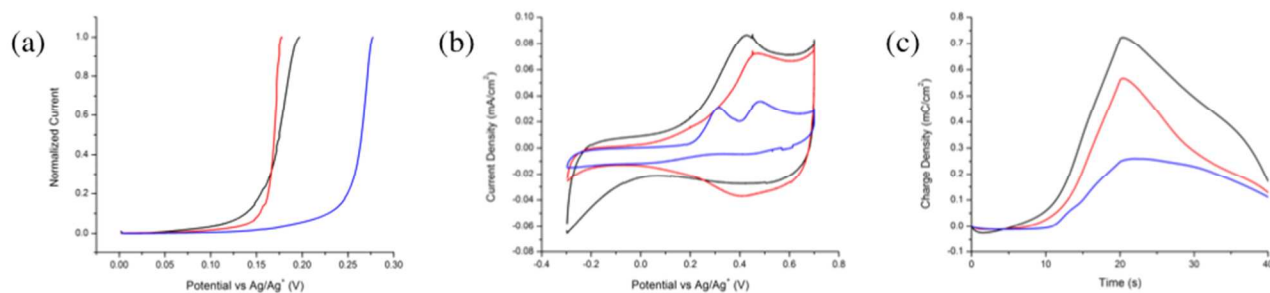
Figure 6. (a) DPV of thin films measured at 5mV/sec. (b) CV (30th scan) of the polymer films from 0-

0.7V vs. Ag/Ag$^+$. (c) Charge passed through the film over the course of the 30th CV scan showing

slow/incomplete reduction. (**pEAE**-black, **pEAAE**-red, **pEABAE**-blue).

Upon examination of the CVs in **Figure 6b**, it becomes evident how similar **pEAE** and **pEAAE**

behave electrochemically with one distinct oxidation. **pEABAE**, on the other hand, has two distinct

oxidations, suggesting further oxidation to a dication. Examination of the charge accumulation results in

Figure 6c, show both processes through a cycle of the CV to be partially irreversible for all polymers.

This finding suggests trapped radical cation states in the film that cannot be fully reduced through

electrochemical means. In order to ensure that the materials were not irreversibly degrading with the

redox chemistry, the films were treated with hydrazine to successfully return them to their original

oxidation state and color (**Figure 7**). **Figure 7a** shows the absorption of **pEAAE** as a pristine film and

the formation of a broad absorption upon oxidation at +750 mV. Upon the application of a reducing

potential of -500 mV for 5 minutes, only some of the original absorption is regained. This can be seen in

Figure 7b as the material changes from a deep blue to a green in color as some low wavelength

absorption returns. Upon removal of the electrodes and subsequent addition of hydrazine it can be seen

from the photographs that the original color of the charge neutral state is returned.
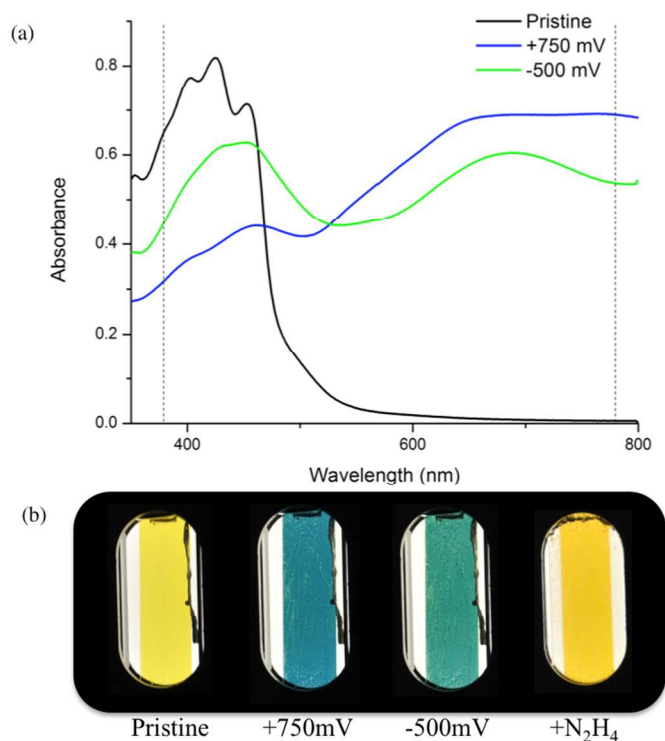
Figure 7. (a) Spectra of **pEAAE** showing the electrochemical irreversibility of the material upon oxidation. (b) Photographs of the same film showing the chemical reversibility of the system upon hydrazine reduction.

This irreversible electrochemical response is a surprising observation based on the high electroactivity of multi-heterocycle, broken conjugation linear polymers and acrylate coatings.[40,43–45] **Figure 8** schematically shows a cross-sectional representation of the polymer at the interface of the electrode. We speculate that, as the polymer film is being oxidized, the chromophore layer closest to the electrode is oxidized first, elevating its conductivity (**Figure 8a**). This increase in conductivity facilitates charge hopping between chromophores through the film, thus oxidizing the bulk (**Figure 8b**). Application of a reducing potential causes this first layer of chromophores to reduce to their neutral, insulating states (**Figure 8c**). This neutral layer acts as an insulating barrier preventing reduction of the remaining charged states in the polymer (**Figure 8d**). These films can be fully reduced back to the neutral with the addition of a chemical reductant, but the fully neutral form cannot be re-obtained based purely on electrochemical reduction (**Figure 8e**). This type of behavior is not useful for typical electrochromic

15

applications, but could have potential use as a visual fuse that switches upon reaching an overpotential.[46–49] This fuse would remain in the new colored state until chemically reduced to the neutral state.
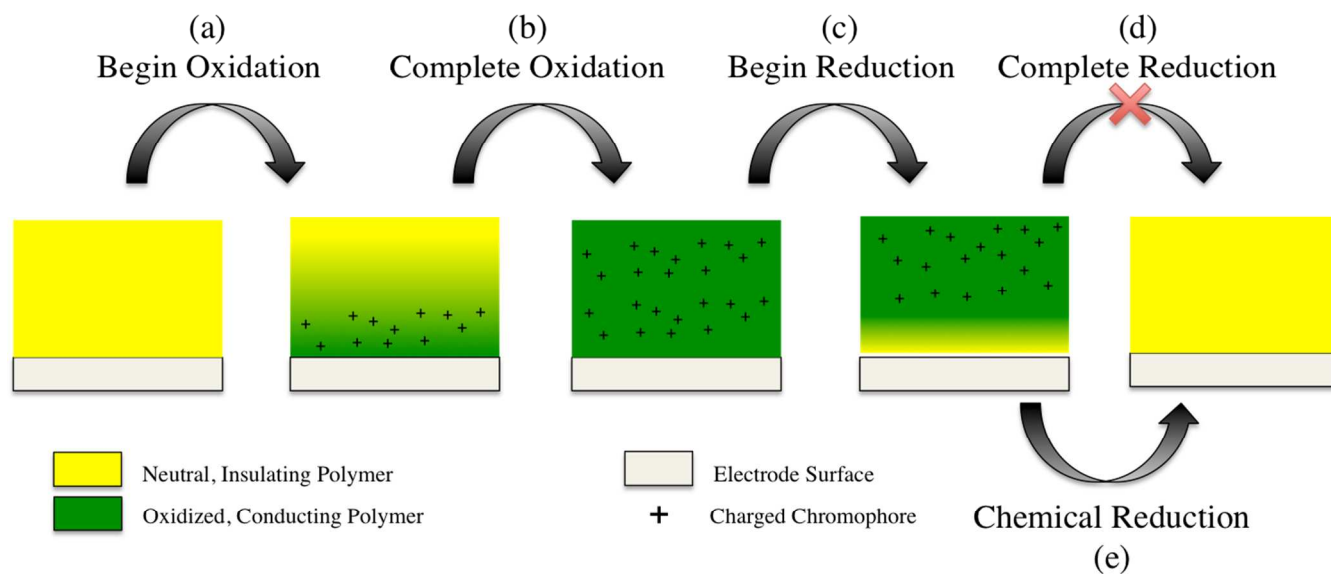
Figure 8. Cross sectional representation of broken conjugation ECP on an ITO glass substrate depicting the charge flow and postulated cause of electrochemical irreversibility. Note the ECP is immersed in electrolyte solution and each charge on the polymer is balanced by an electrolyte anion (PF_6^-).

The energy and width of the radical cation absorption spectra and how the switching potentials can be tuned as they relate to the chromophores' structures are important in understanding these types of systems. To this end, we examine the absorption properties of these polymers. The UV/Vis spectra of the polymers were measured in a solution of 40 µg/ml in dichloromethane (DCM), normalized for **Figure 9a**. Contrary to the DFT calculations there is a red-shifting of the chromophores' absorbances increasing the conjugation of the dioxythiophene chromophores with λ_{max} for **pEAE** and **pEAAE** being 386nm and 424nm, respectively. However, due to the large steric strain between the AcDOTs and dimethoxybenzene in **pEABAE**, the chromophore is twisted thereby lowering the extent of conjugation and a lower λ_{max} of 395nm.

To probe the spectral changes of the polymers during oxidation, films were spray coated onto ITO/glass using a hand-held airbrush from 3 mg/mL polymer-toluene solutions to an absorbance of 0.8-1.0 AU. As can be seen in **Figure 9b**, the normalized absorbance for the all of the polymers is largely unchanged relative to the solution spectra, other than peak broadening. This broadening is more significant in the case of **pEABAE** causing it to adopt an absorption onset closer to that of **pEAAE**.
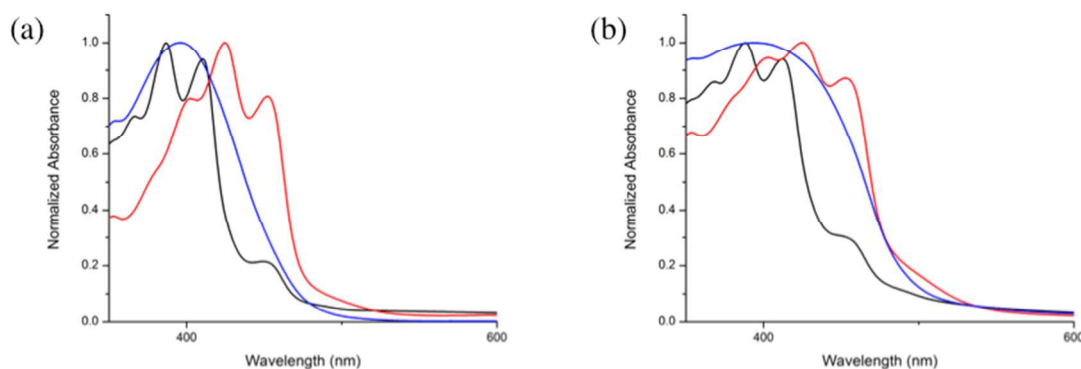

Figure 9. (a) Normalized solution UV/Vis absorbances of the polymers. (b) Normalized thin film absorbances of the polymers. (**pEAE**-black, **pEAAE**-red, **pEABAE**-blue). It can be seen that the absorption onset for these materials is redshifted moving to the solid state with a greater degree of broadening for **pEABAE** indicative of more chromophore-chromophore aggregation.

Film Spectroelectrochemistry and Colorimetry. Spectroelectrochemical measurements were performed in 0.5 M TBAPF$_6$ in propylene carbonate with a platinum counter electrode and a Ag/Ag$^+$ reference electrode as shown in **Figure 10** along with photographs of the films held at potential extremes dictated by the CVs results. As a pristine film, **pEAE** shown in **Figure 9a** absorbs at a λ_{max} of 386 nm (i) capturing only a small portion of the visible giving a pale yellow color. Oxidation of **pEAE** to the radical cation state reduces the intensity of peak 'i' and gives rise to a sharp absorbance with at λ_{max} 582 nm (ii) centered in the visible with a less intense peak in the near IR at 935 nm (iii). This new oxidation state is perceived as blue as the lower energy red and green light is absorbed and blue is transmitted.

Turning attention to **Figure 10b** the neutral absorbance of **pEAAE** is redshifted compared to **pEAE** with a λ_{max} at 424 nm (iv), thus absorbing more blue light and creating a deeper yellow color. Upon oxidation of **pEAAE**, the neutral peak 'iv' reduces in intensity and the polymer radical cation begins to absorb in the visible at λ_{max} at 687 nm (v) and in the near IR at 1050 nm (vi), both redshifted compared to **pEAE** as predicted by calculations. Upon further oxidation, peak 'v' begins to decrease in intensity with the continued growth of a broadly absorbing peak 'vi' in the near-IR indicative of a dication species. This charged state has some absorbance of lower energy red light, allowing more green and blue light to transmit, and is perceived as a teal-turquoise color.

With increasing conjugation it was expected that **pEABAE** would have a neutral peak red-shifted compared to the two shorter chromophores, but the steric repulsion between the dimethoxybenzene and AcDOTs cause a decrease of π overlap in the center of the chromophore, widening the optical gap, and giving rise to an absorption with λ_{max} at 395 nm (vii). This absorbance profile yields a film that is similar in appearance to that of **pEAAE**. Upon oxidation of **pEABAE** there is the growth of two sharp and intense peaks with λ_{max} at 450 nm (viii) and 587 nm (ix). The combined absorbance of these peaks allows for this charged state absorption to encompass a large portion of the visible range causing the film to appear as a dark black. Note that the intensity of the absorbance in this material's oxidized state is much higher than that of the neutral state. We postulate that this large increase in intensity and the high energy of the absorptions compared to the all dioxythiophene chromophores are likely from two different radical cation species or the formation of radical cation aggregates.
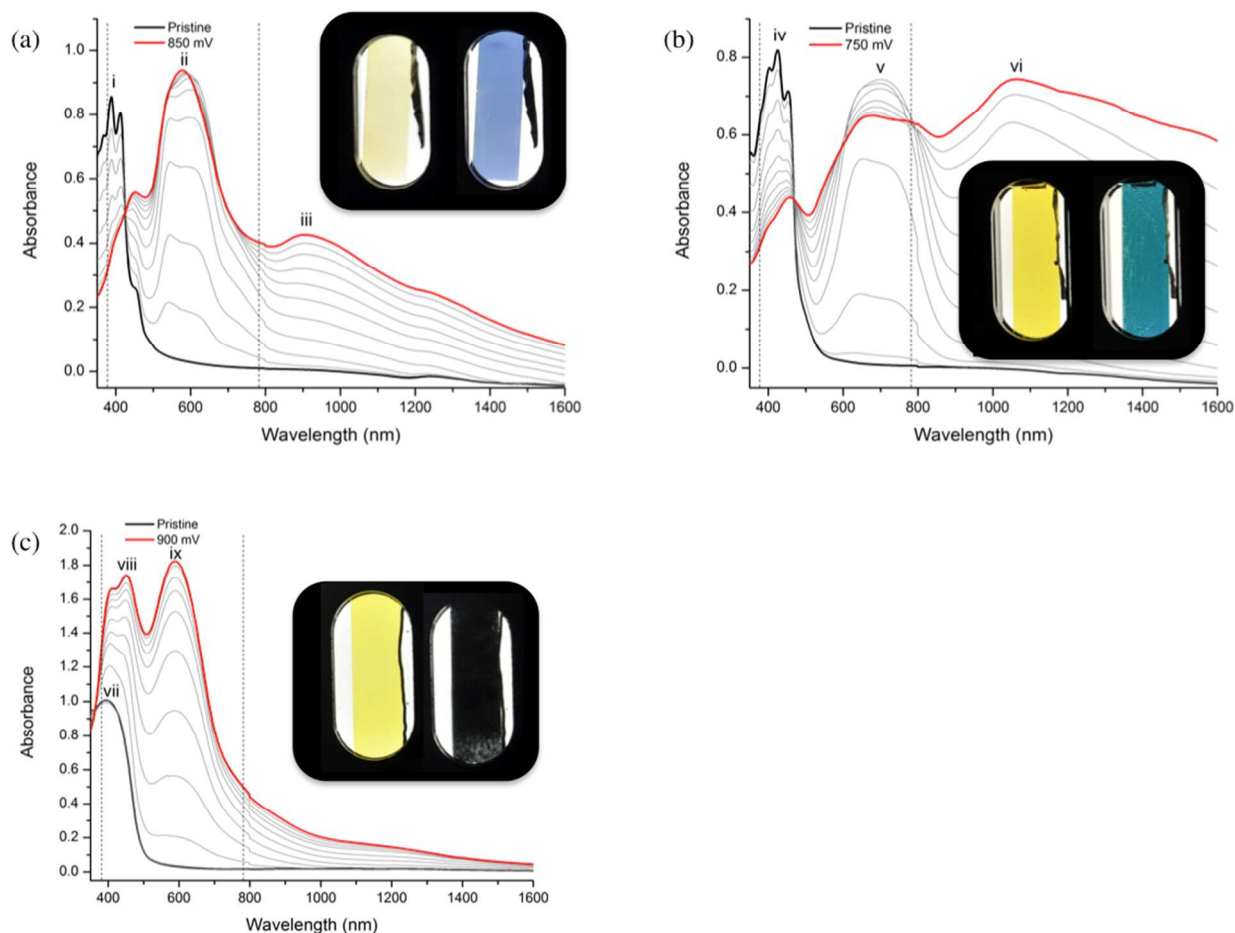
Figure 10. Spectroelectrochemistry of polymer films on ITO-glass in 0.5 M TBAPF$_6$-PC with potential steps of 50 mV from the pristine (black trace) to the fully oxidized form (red trace). Photographs of each polymer (left – as cast, right – oxidized) are in the insets of each representative spectrum (**pEAE** (a), **pEAAE** (b), **pEABAE** (c))

Colorimetry. The L*a*b* color space results for the polymers under study are presented graphically in **Figure 11** with the values collated in Table 2. In this color space, positive a*and b* represents red and yellow while the negative values indicate blue and green, respectively. As the magnitudes of a* and b* increase, the color becomes more saturated, and as one traverses between color points, the hue changes. L* depicts the lightness: a value of 0 would be black and 100 would be white.

In the neutral state, **pEAE** is a low saturation yellow (b* = 26) with a high lightness value (L* = 96), due to the minimal absorbance tailing into the high-energy side of the visible spectrum. Comparatively,

pEAAE and pEABAE have L* and a* values similar to pEAE, but are much more saturated (higher

b*) observed by their more intense yellow color. Upon oxidation, pEAE passes through the origin along

the b* axis to create a blue radical cation state with a similar saturation to that of the neutral form with a

much lower L* value, 45. pEAAE follows the formation of a green radical cation state with a largely

negative a* value, and upon further oxidation the color coordinates move towards the origin to make a

low saturation blue-green color at 750mV. For pEABAE the formation of the two radical species causes

the loss of color saturation and an oxidized state with color coordinates close to the origin (colorless).

The L* value dropping to 18 indicates a low percentage of light transmitting across the visible. This

appears to the eye as a dark, black film.
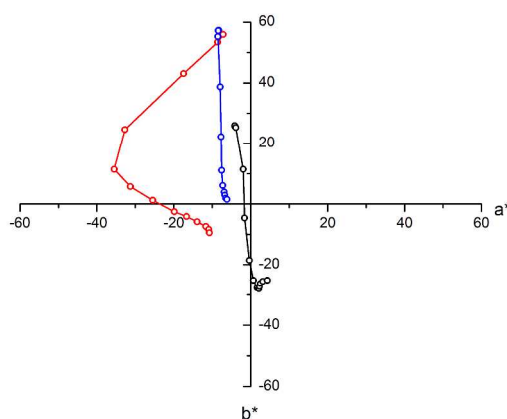
Figure 11. Progression of L*a*b* color coordinates of polymer films from pristine to oxidized (pEAE-

black, pEAAE-red, pEABAE-blue).

Table 2 . Color coordinate values for the pristine and oxidized states of the polymer films.

	Pristine	Radical Cation
Polymer	L*, a*, b*	L*, a*, b*
pEAE	96, -4, 26	45, 4, -25
pEAAE	96, -7, 56	64, -12, -7
pEABAE	95, -8, 57	18, -6, 1

Charge State Elucidation of pEABAE. In the spectroelectrochemistry for **pEABAE** the charged state exhibited an unusually high-energy absorption characteristic compared to what was calculated. To elucidate the unusual charge state for this chromophore, computational methods were utilized. For this calculation, the chromophore is broken into pieces with the idea that the dimethoxybenzene would act as a steric block in the conjugation of the radical cation. **Figure 12** shows calculated radical cation state absorptions of segmented portions of the **EABAE** chromophore overlaid with the experimental spectroelectrochemistry. These calculations suggest that there are two main phenomena contributing to the radical cation spectra: twisted/conjugation broken chromophores and π-π stacking. As demonstrated by the frontier molecular orbitals in **Figure 4**, the computations strongly support that the two experimental peaks at 412 nm and 452 nm are contributions from the two-ring dioxythiophene portions of the chromophore (**EA**, 405 nm) and the three-ring fraction (**EAB**, 456 nm), respectively. Surprisingly, the results did not support any major influences from the full chromophore (**EABAE**, 496 nm). In an effort to identify the contributor(s) to the 587 nm peak, a radical cation π-dimer comprised of **EA** and **EAB** units (**Figure S3n**) was generated. This aggregate, producing a 562 nm peak, provides strong support that intermolecular π-π stacking is likely responsible for the low energy peak.[50–53] Other combinations were also examined, but were unable to produce optimized aggregates and therefore require further studies.
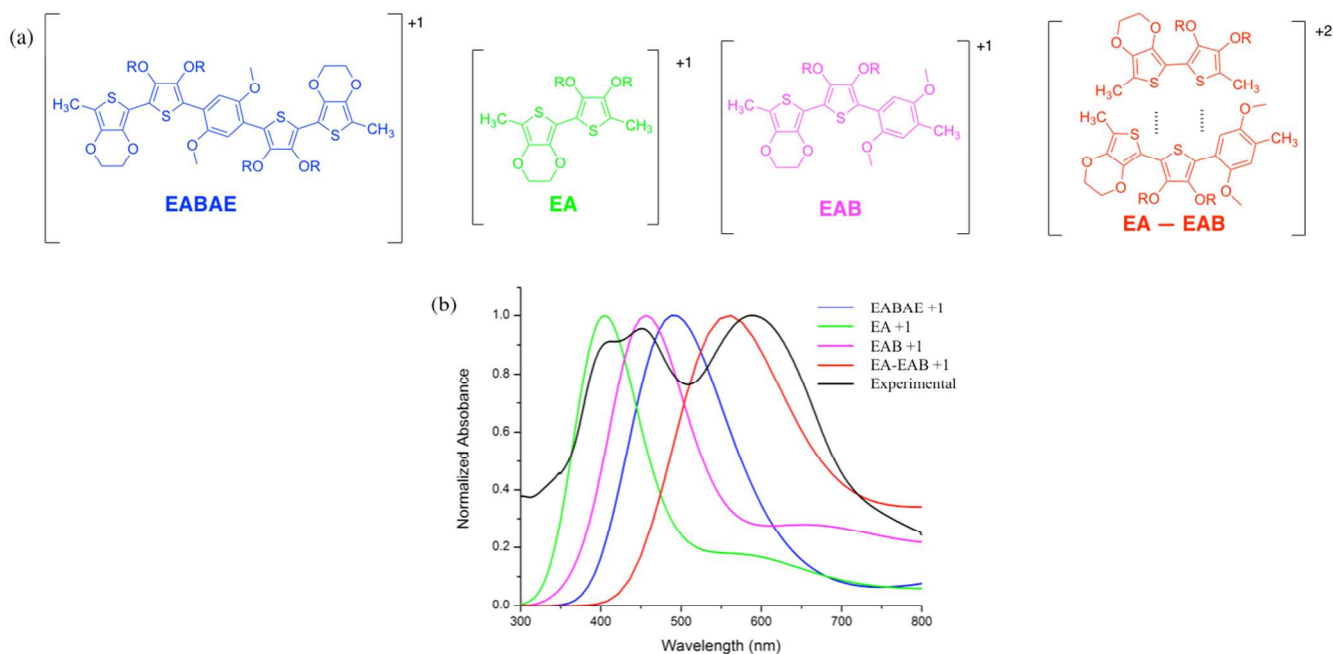
Figure 12 – (a) Structures indicating where the steric blocks in the structure may occur for limiting the radical cation delocalization. These structures' absorptions were calculated to simulate a radical that is localized. **EA-EAB** is the π face interaction of the radical cation state of two portions of separate molecules (b) Calculated radical cation state absorptions of the segmented portions of the **EABAE** chromophore compared to the experimental data.

CONCLUSIONS AND PERSPECTIVE

The contrast challenge for cathodically coloring electrochromics is examined from a fundamental standpoint leading to the determination that anodically coloring materials provide a means to conquer the issue. Here, we focused on examining the design principles of creating chromophores with discrete lengths and varying amounts of strain. Theoretical calculations, coupled with design and synthesis, helped to elucidate the interplay between sterics and chromophore size. Inter-ring steric interactions, leading to large dihedral angles, can be used as a conjugation wedge to limit, not only the neutral absorption, but also the delocalization of charged states creating radical cations that absorb at high energies compared to chromophores of similar size, but less steric encumbrance. The use of steric interactions as a conjugation block also gives the advantage of forming multiple and different high-

energy light absorbing charged states. Considering the broad absorption achieved by the apparent dimerization of the **EABAE** chromophore attention should be shifted towards designing molecules for this purpose. The electrochemical irreversibility does appear to be a problem for purely electrochromic applications, but it does however appear to offer an interesting approach toward making materials that could be used as overpotential fuses.

EXPERIMENTAL SECTION

Synthetic Procedures

pEAE. Into a dry 25 mL schlenk tube with magnetic stirring was added the dibromide monomer **BrABr** (0.154 g, 0.308 mmol), the dihydrin monomer **E~E** (0.100g, 0.308 mmol), 2 mol% palladium acetate (1.5 mg, 0.007 mmol), pivalic acid (0.031 g, 0.304 mmol), potassium carbonate (0.138 g, 0.997 mmol), and 3.1 mL of DMAc. The reaction mixture was purged with Ar, placed in an oil bath at 130°C, and stirred for 24 hours under positive Ar pressure. The mixture was cooled to room temperature and added drop wise to 100 mL of methanol. The precipitate was filtered through a Soxhlet thimble, and washed with methanol, acetone, hexanes, and chloroform respectively. The washings were conducted until color was no longer observed during extraction. The solvent was evaporated from the fraction and a pale-yellow solid was collected (0.1004g, 49.3%). ^{1}H-NMR (CDCl$_3$, ppm): δ 4.29-4.20 (d, 8H), 3.93-3.90 (d, 4H), 2.72 (t, 4H), 1.96-1.84 (bm, 4H), 1.59~1.25 (bm, 16H), 0.91~0.87 (bm, 12H). Elemental analysis: Theory: C= 63.60%, H=7.32%, S=14.55%, Found: C= 63.38%, H=7.37%, S=14.28%. GPC analysis: M$_n$= 14.8 kDa, Đ = 2.0.

pEAAE. The polymer was synthesized using the same procedure as **pEAE**, but with the dibromide monomer **BrAABr** (0.258 g, 0.308 mmol). The polymer was collected as a yellow solid (0.1638 g, 53.2%). ^{1}H-NMR (CDCl$_3$, ppm): δ 4.20-4.14 (d, 8H), 3.87-3.85 (d, 8H), 2.66 (t, 4H), 1.85 (m, 6H), 1.64-1.02 (bm, 32H), 0.98~0.58 (bm, 24H). Elemental analysis: Theory: C= 66.09%, H=8.27%, S=12.83%, Found: C= 65.63%, H=8.29%, S=12.50%. GPC analysis: M$_n$= 18.5 kDa, Đ = 1.8.

pEABAE. The polymer was synthesized using the same procedure as **pEAE**, but with the dibromide monomer **BrABABr** (0.300 g, 0.308 mmol). The polymer was collected as a yellow solid (0.1705 g, 48.7%). ^{1}H-NMR (CDCl$_3$, ppm): δ 7.37 (s, 2H), 4.29-4.22 (d, 8H), 3.97 (d, 4H), 3.84 (bm, 10H), 2.75-2.72 (q, 4H), 1.64-1.02 (bm, 32H), 0.98~0.58 (bm, 24H). Elemental analysis: Theory: C= 66.63%, H=7.99%, S=11.29%, Found: C= 66.40%, H=7.99%, S=11.05%. GPC analysis: M$_n$= 9.7 kDa, Đ = 2.0.

Instrumentation. ^{1}H NMR and ^{13}C NMR spectra were collected on a Varian Mercury Vx 300 MHz instrument using CDCl$_3$ as a solvent and the residual CHCl$_3$ peak as references (^{1}H: δ = 7.26 ppm; ^{13}C: δ = 77.23 ppm). Gel permeation chromatography (GPC) was performed using a Tosoh EcoSEC HLC-8320 GPC at 40 °C in chloroform. A TSKgel column (4.6 mm × 150 mm) and PStQuick polystyrene standards from Tosoh were used. Polymer solutions (1 mg/mL in CHCl$_3$) were prepared and filtered through a PTFE 0.45 μm filter. 20 μL of each polymer solution was injected, and molecular weights were calculated using EcoSEC GPC System Workstation Software. All absorption spectra and spectroelectrochemistry were acquired using a Varian Cary 5000 Scan dual-beam UV−vis−near-IR spectrophotometer. Colorimetry measurements were obtained using Star-Tek colorimetry software using a D50 illuminant, 2 deg observer, and the L*a*b* color space. For the solution spectra, all polymers were dissolved in toluene at room temperature. Electrochemical measurements were carried out using an EG&G Princeton Applied Research model 273A potentiostat/galvanostat under CorrWare control in a three-electrode cell configuration, using ITO/glass (Delta Technologies Inc., 7 × 50 × 0.7 mm, sheet resistance, Rs 8−12 Ω/sq) as the working electrode, a Ag/Ag$^+$ reference electrode (10 mM AgNO$_3$ in 0.5 M TBAPF$_6$−propylene carbonate (PC), E$_{1/2}$ for ferrocene: 0.125 V), and a Pt flag as the counter electrode. For differential pulse voltammetry (DPV) measurements, the samples were prepared via drop-casting a 0.5 mg/ mL solution onto glassy carbon button electrode with a surface area of 0.07 cm^2. An electrolyte solution of 0.5 M TBAPF$_6$ (98%, purified via recrystallization from hot ethanol) in PC was used in all electrochemical and spectroelectrochemical measurements. PC was purified using a solvent

purification system from Vacuum Atmospheres. ITO coated glass slides were cleaned with toluene, acetone, and isopropanol prior to use and implemented as the working electrode for the spectroelectrochemical measurements. Films were spray-cast onto the ITO-coated glass slides using an Iwata airbrush at 25 psi from 3 mg/mL toluene solutions. Photography was performed in a light booth designed to exclude outside light with a D50 (5000K) lamp located in the back of the booth providing illumination, using a Nikon D90 SLR camera with a Nikon 18-105 mm VR lens.

Materials. Most reagents and starting materials were purchased from commercial sources and used without further purification, unless otherwise noted. THF, toluene, and propylene carbonate were all purified through a Bruker or Vacuum Atmospheres solvent purification system. 2,5-dibromo-3,4-bis(2-ethylhexyloxy)thiophene (**BrABr**), 2,5'-dibromo-3,3',4,4'-tetrakis((2-ethylhexyl)oxy)-2,2'-bithiophene (**BrAABr**), and **BrABABr** were used as synthesized in previous literature.[54,55]

ACKNOWLEDGEMENTS

REFERENCES

1   R. J. Mortimer, *Annu. Rev. Mater. Res*, 2011, **41**, 241–68.

2   J. Rivnay, *Nat Mater*, 2016, **15**, 594–595.

3   A. Teichler, J. Perelaer and U. S. Schubert, *J. Mater. Chem. C*, 2013, **1**, 1910–1925.

4   R. R. Søndergaard, M. Hösel and F. C. Krebs, *J. Polym. Sci. Part B Polym. Phys.*, 2013, **51**, 16–34.

5   Z. B. Henson, K. Müllen and G. C. Bazan, *Nat. Chem.*, 2012, **4**, 699–704.

6   J. Mei, Y. Diao, A. L. Appleton, L. Fang and Z. Bao, *J. Am. Chem. Soc.*, 2013, **135**, 6724–6746.

7   H. Zhou, L. Yang and W. You, *Macromolecules*, 2012, **45**, 607–632.

8   G. Li, R. Zhu and Y. Yang, *Nat. Photonics*, 2012, **6**, 153–161.

9   A. L. Dyer, E. J. Thompson and J. R. Reynolds, *ACS Appl. Mater. Interfaces*, 2011, **3**, 1787–1795.

10   P. Shi, C. M. Amb, E. P. Knott, E. J. Thompson, D. Y. Liu, J. Mei, A. L. Dyer and J. R. Reynolds, *Adv. Mater.*, 2010, **22**, 4949–4953.

11   R. H. Bulloch, J. A. Kerszulis, A. L. Dyer and J. R. Reynolds, *ACS Appl. Mater. Interfaces*, 2015, **7**, 1406–1412.

12   A. M. Osterholm, D. E. Shen, J. A. Kerszulis, R. H. Bulloch, M. Kuepfert, A. L. Dyer and J. R. Reynolds, *ACS Appl. Mater. Interfaces*, 2015, **7**, 1413–1421.

13   S. Abraham, S. Mangalath, D. Sasikumar and J. Joseph, *Chem. Mater.*, 2017, **29**, 9877–9881.

14   H. Shin, Y. Kim, T. Bhuvana, J. Lee, X. Yang, C. Park and E. Kim, *ACS Appl. Mater. Interfaces*, 2012, **4**, 185–191.

15   H.-J. Yen, K.-Y. Lin and G.-S. Liou, *J. Mater. Chem.*, 2011, **21**, 6230–6237.

16   G. Ding, C. M. Cho, C. Chen, D. Zhou, X. Wang, A. Y. X. Tan, J. Xu and X. Lu, *Org. Electron.*, 2013, **14**, 2748–2755.

17   T. Jarosz, A. Brzeczek, K. Walczak, M. Lapkowski and W. Domagala, *Electrochim. Acta*, 2014, **137**, 595–601.

18   O. Bubnova and X. Crispin, *Energy Environ. Sci.*, 2012, **5**, 9345–9362.

19   P. M. Beaujuge, C. M. Amb and J. R. Reynolds, *Chem. Rev.*, 2010, **110**, 268–320.

20   Y. Li and T. Michinobu, *J. Polym. Sci. Part A Polym. Chem.*, 2012, **50**, 2111–2120.

21   W. H. Nguyen, C. J. Barile and M. D. McGehee, *J. Phys. Chem. C*, 2016, **120**, 26336–26341.

22   C. G. Granqvist, *Thin Solid Films*, 2014, **564**, 1–38.

23   R. J. Mortimer, A. L. Dyer and J. R. Reynolds, *Displays*, 2006, **27**, 2–18.

24   M. Sezgin, O. Ozay, S. Koyuncu, H. Ozay and F. Baycan Koyuncu, *Chem. Eng. J.*, 2015, **274**, 282–289.

25   A. A. Argun, P.-H. Aubert, B. C. Thompson, I. Schwendeman, C. L. Gaupp, J. Hwang, N. J. Pinto, D. B. Tanner, A. G. MacDiarmid and J. R. Reynolds, *Chem. Mater.*, 2004, **16**, 4401–4412.

26   P. Camurlu, *RSC Adv.*, 2014, **4**, 55832–55845.

27   J.-T. Wu and G.-S. Liou, *Chem. Commun.*, 2018, **54**, 2619–2622.

28   H.-S. Liu, B.-C. Pan, D.-C. Huang, Y.-R. Kung, C.-M. Leu and G.-S. Liou, *NPG Asia Mater.*, 2017, **9**, e388.

29   D. Weng, Y. Shi, J. Zheng and C. Xu, *Org. Electron.*, 2016, **34**, 139–145.

30   G. Tahtali, Z. Has, C. Doyranli, C. Varlikli and S. Koyuncu, *J. Mater. Chem. C*, 2016, **4**, 10090–10094.

31   S.-H. Hsiao, G.-S. Liou, Y.-C. Kung and H.-J. Yen, *Macromolecules*, 2008, **41**, 2800–2808.

32   G. Sönmez, I. Schwendeman, P. Schottland, K. Zong and J. R. Reynolds, *Macromolecules*, 2003, **36**, 639–647.

33   R. M. Walczak and J. R. Reynolds, *Adv. Mater.*, 2006, **18**, 1121–1131.

34   C. Mortier, T. Darmanin and F. Guittard, *Macromolecules*, 2015, **48**, 5188–5195.

35   G. Kurtay, T. Soganci, M. Ak and M. Gullu, *J. Electrochem. Soc.*, 2016, **163**, 896–905.

36   E. P. Knott, M. R. Craig, D. Y. Liu, J. E. Babiarz, A. L. Dyer and J. R. Reynolds, *J. Mater. Chem.*, 2012, **22**, 4953–4962.

37   F. A. Arroyave and J. R. Reynolds, *Macromolecules*, 2012, **45**, 5842–5849.

38   H.-J. Yen and G.-S. Liou, *Polym. Chem.*, 2012, **3**, 255–264.

39   H. J. Yen, C. J. Chen and G. S. Liou, *Adv. Funct. Mater.*, 2013, **23**, 5307–5316.

40   R. Stalder, A. Mavrinskiy, C. Grand, W. Imaram, A. Angerhofer, W. Pisula, K. Müllen and J. R. Reynolds, *Polym. Chem.*, 2015, **6**, 1230–1235.

41   K. Nawa, I. Imae, N. Noma and Y. Shirota, *Macromolecules*, 1995, **28**, 723–729.

42   D. L. Wheeler, L. E. Rainwater, A. R. Green and A. L. Tomlinson, *Phys. Chem. Chem. Phys.*, 2017, **19**, 20251–20258.

43   C. B. Nielsen, A. Angerhofer, K. A. Abboud and J. R. Reynolds, *J. Am. Chem. Soc.*, 2008, **130**, 9734–9746.

44   J. Y. Oh, S. Rondeau-Gagné, Y.-C. Chiu, A. Chortos, F. Lissel, G.-J. N. Wang, B. C. Schroeder, T. Kurosawa, J. Lopez, T. Katsumata, J. Xu, C. Zhu, X. Gu, W.-G. Bae, Y. Kim, L. Jin, J. W. Chung, J. B.-H. Tok and Z. Bao, *Nature*, 2016, **539**, 411–415.

45   S. Savagatrup, X. Zhao, E. Chan, J. Mei and D. J. Lipomi, *Macromol. Rapid Commun.*, 2016, **37**, 1623–1628.

46   J. Janata, *Principles of chemical sensors*, Springer Science & Business Media, 2010.

47   M. C. Gallazzi, L. Tassoni, C. Bertarelli, G. Pioggia, F. Di Francesco and E. Montoneri, *Sensors Actuators B Chem.*, 2003, **88**, 178–189.

48   R. Rella, P. Siciliano, F. Quaranta, T. Primo, L. Valli and L. Schenetti, *Colloids Surfaces A*

Physicochem. Eng. Asp., 2002, **198–200**, 829–833.

49   M. F. Mabrook, C. Pearson and M. C. Petty, *Appl. Phys. Lett.*, 2004, **86**, 13507.

50   D. A. Scherlis and N. Marzari, *J. Phys. Chem. B*, 2004, **108**, 17791–17795.

51   M. G. Hill, J. F. Penneau, B. Zinger, K. R. Mann and L. L. Miller, *Chem. Mater.*, 1992, **4**, 1106–1113.

52   P. Hapiot, P. Audebert, K. Monnier, J.-M. Pernaut and P. Garcia, *Chem. Mater.*, 1994, **6**, 1549–1555.

53   G. Zotti, G. Schiavon, A. Berlin and G. Pagani, *Chem. Mater.*, 1993, **5**, 620–624.

54   K. Cao, D. E. Shen, A. M. Osterholm, J. A. Kerszulis and J. R. Reynolds, *Macromolecules*, 2016, **49**, 8498–8507.

55   J. A. Kerszulis, C. M. Amb, A. L. Dyer and J. R. Reynolds, *Macromolecules*, 2014, **47**, 5462–5469.

TOC image and sentence:
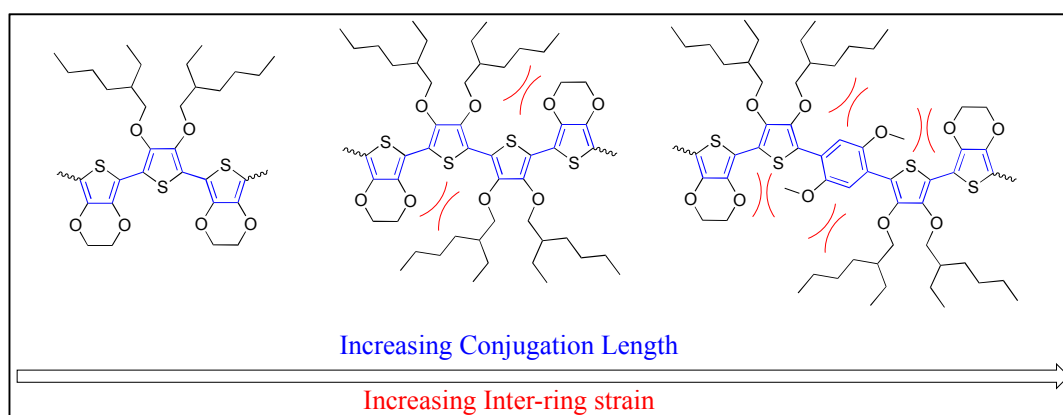
This paper details the theoretical calculations, synthesis, and electrochromism of polymeric materials consisting of conjugated chromophores separated by nonconjugated linkers.